Structural Engineering and Mechanics, Vol. 3, No. 4 (1995) 325-340
DOI: http://dx.doi.org/10.12989/sem.1995.3.4.325

Elasto-plastic nonconforming solid element with variable nodes

Chang-Koon Choi† and Gi-Taek Chung‡

Department of Civil Engineering, Korea Advanced Institute of Science and Technology, Taejon 305-701, Korea

Abstract. The iterative procedure to use the nonconforming elements in elasto-plastic problems is established and applied to the variable node transition solid element developed for the automated three-dimensional local mesh refinement. Through numerical tests, the validity and performance of the element are examined. As the nonlinear iterative procedure presented in this paper is accomplished for the general three-dimensional case, it can also be easily applied to the two-dimensional elements such as membranes, plates and shells.

Key words: elasto-plastic analysis; mesh refinement; nonconforming modes; steep stress gradient; super-convergent patch recovery; transition solid element; variable node; yield propagation

1. Introduction

Fully three-dimensional analysis embraces clearly all the practical engineering problems. It is obvious, however, that the number of degrees-of-freedom necessary to achieve a given degree of accuracy by the three-dimensional analysis has to be very large. It is not surprising therefore that efforts to improve accuracy of the analysis by the use of more complex elements have been strongest in the area of three-dimensional analysis (Spilker and Singh 1982, Gupta 1984, Yunus, *et al.* 1991, Smith and Kidger 1992, Chen and Cheung 1992).

The eight-node hexahedron solid element has been frequently used in the three-dimensional structural analysis due to its simplicity and easy availability. However, when a complicated structure needs to be gradually refined locally and reanalyzed due to the existence of steep stress gradient and/or the singularity due to the concentrated local load, the overall mesh should be reconstructed to be consistent with the local stress gradient. For such mesh gradation, the use of eight-node solid elements often leads either to meshes with highly distorted elements or to meshes with too many degrees-of-freedom which may exceed the economical limit of computation.

A new solid element with variable nodes was established to be used effectively as transition elements in three-dimensional modeling (Choi and Lee 1993). The improvement achieved by the addition of the nonconforming modes was significant and the use of this type of element in modeling transition zone is very effective and stable. To date, however, the application of this element has been limited to the problems within elastic domain. In this paper, the use of nonconforming transition solid element is extended to the materially nonlinear problems. The formulation of the element is briefly reviewed and an iterative procedure to add material

† Professor
‡ Graduate Student

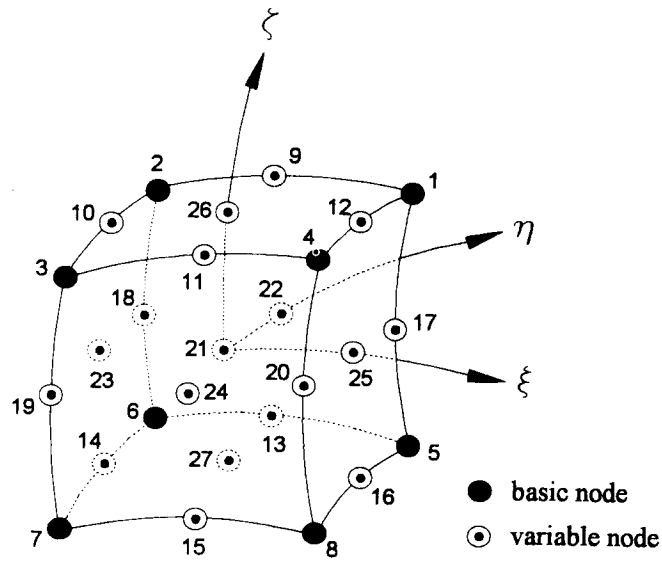

Fig. 1 Transition element with variable nodes from 8 to 27.

nonlinearity to the nonconforming element is suggested in subsequent sections. Through the numerical tests, the validity and performance of the proposed element is examined.

2. Nonconforming transition solid element

For the automated three-dimensional local mesh refinement where the steep stress gradient exists, a three-dimensional transition solid element has been developed by Choi and Lee (1993). The developed transition element was established by adding a variable number of nodes to the basic nonconforming 8-node solid element (NC8) for an effective connection between the refined region and the coarse region with minimum degrees of freedom possible. Based on the basic configuration and the node numbering of the element, a series of new solid transition elements which have up to 27 nodes can be systematically established (Fig. 1). The basic behavior of these elements has been improved through the addition of modified nonconforming displacement modes.

It was verified by Choi and Lee (1993) that the developed elements passed the patch test and there are no spurious zero energy mechanisms. Moreover, in case of the highly distorted mesh, the accuracy of the nonconforming elements is markedly better than that of the conventional elements.

The general displacement approximations for the variable-node element with the nonconforming modes which are modified to incorporate the contributions of variable nodes are of the form

$$\boldsymbol{u}=\boldsymbol{N}_c\boldsymbol{u}_c+\boldsymbol{N}_n\boldsymbol{u}_n \tag{1}$$

where c indicates conforming, n indicates nonconforming, $\boldsymbol{u}_c$ is the nodal displacement vector, $\boldsymbol{u}_n$ is the nonconforming mode interpolation parameter vector, $\boldsymbol{N}_c$ is the compatible interpolation

functions, and N_n is the corresponding nonconforming modes modified from those of a regular hexahedron element to consider the nature of variable nodes that a transition element has. The derived shape functions and the detailed formulation for the element can be found in Choi and Lee (1993).

Then the element strains are given as

$$\varepsilon = B_c u_c + B_n u_n \tag{2}$$

where strain-displacement matrices B_c and B_n are obtained by differentiating the shape functions N_c and N_n, respectively, imposing constraints as described by Choi and Lee (1993).

The augmented equilibrium equation in a matrix form due to the addition of the nonconforming displacement modes u_n is given as (Choi and Park 1989)

$$\begin{bmatrix} K_{cc} & K_{cn} \\ K_{cn}^T & K_{nn} \end{bmatrix} \begin{Bmatrix} u_c \\ u_n \end{Bmatrix} = \begin{Bmatrix} f \\ 0 \end{Bmatrix} \tag{3}$$

where

$$K_{cc} = \int_V B_c^T D B_c \, dV \tag{4}$$

$$K_{cn} = \int_V B_c^T D B_n \, dV \tag{5}$$

$$K_{nn} = \int_V B_n^T D B_n \, dV \tag{6}$$

in which D is the general (6×6) stress-strain matrix. It is noted that the lower part of force vector contains only zeros since the nonconforming modes (u_n) are not physical nodal displacements and accordingly the corresponding force terms cannot be defined.

Through the static condensation, Eq. (3) is modified to give the final equilibrium equation

$$\bar{K} u_c = f \tag{7}$$

where $\bar{K}$ is condensed back to the original matrix size and given as

$$\bar{K} = K_{cc} - K_{cn} K_{nn}^{-1} K_{cn}^T. \tag{8}$$

The newly established element has been designated as NCV (NonConforming Variable node element) in this study.

3. Nonconforming element in inelastic problems

Although there have been quite a few recent researches on the development of the finite elements with nonconforming displacement modes (Choi and Park 1989, Wilson and Ibrahimbegovic 1990, Choi and Lee 1993), the use of these elements in structural analysis with material nonlinearity is seldom found in the published literature. The main difficulty associated with utilizing the nonconforming finite elements in materially nonlinear analysis is that these elements include the nonconforming displacement modes in addition to the compatible nodal displacements. When u_n in Eq. (2) is condensed out, the strains of nonconforming elements are estimated

by $\boldsymbol{u}_c$ only

$$\varepsilon=\bar{\boldsymbol{B}}\boldsymbol{u}_c \tag{9}$$

where $\bar{\boldsymbol{B}}$ is the condensed strain-displacement matrix given as

$$\bar{\boldsymbol{B}}=\boldsymbol{B}_c-\boldsymbol{B}_n\boldsymbol{K}_{nn}^{-1}\boldsymbol{K}_{cn}^{T}. \tag{10}$$

This equation reveals that the strain-displacement relationship for nonconforming elements depends partly on the stiffness which includes material property, as well as on the geometry. The materially nonlinear analysis is carried out by the Newton Raphson method with loads applied in several steps. The converged solution in each load step is obtained through the iterative procedure by updating the tangential stiffness $\boldsymbol{K}_{ep}$ in accordance with the flow rule. Therefore, the element strain for nonconforming elements is a function of the $\boldsymbol{K}_{ep}$ matrix rather than a constant. The nonlinear iterative procedure with nonconforming elements in one load step is suggested as follows.

The incremental strains are estimated first from the incremental displacements using the tangential stiffness $\boldsymbol{K}_{ep}^{r}$ as used in the calculation of the incremental displacements

$$d\varepsilon^{r}=\bar{\boldsymbol{B}}^{r}d\boldsymbol{u}^{r} \tag{11}$$

where

$$\bar{\boldsymbol{B}}^{r}=\boldsymbol{B}_c-\boldsymbol{B}_n[\boldsymbol{K}_{nn}^{r}]^{-1}[\boldsymbol{K}_{cn}^{r}]^{T} \tag{12}$$

in which the superscript r is the current iteration in the load step.

Based on these incremental strains, the stresses σ^{r} satisfying the flow rule are determined as

$$\sigma^{r}=\sigma^{r-1}+\boldsymbol{D}d\varepsilon^{r}-d\lambda\boldsymbol{d}_D. \tag{13}$$

The details related to this equation and the flow rule employed in this study can be referred to Appendix.

The final process in the iterative procedure is to calculate the internal forces and check the convergence criterion. For the estimation of the internal forces which are statically equivalent to the current stress field σ^{r}, the tangential stiffness $\boldsymbol{K}_{ep}^{r+1}$ newly updated according to the flow rule is used as

$$\boldsymbol{f}^{r}=\int_V[\bar{\boldsymbol{B}}^{r+1}]^{T}\sigma^{r}dV \tag{14}$$

where

$$\bar{\boldsymbol{B}}^{r+1}=\boldsymbol{B}_c-\boldsymbol{B}_n[\boldsymbol{K}_{nn}^{r+1}]^{-1}[\boldsymbol{K}_{cn}^{r+1}]^{T}. \tag{15}$$

It is noted that terms with the superscript $r+1$ in Eq. (15) will be used to calculate the next incremental displacements $d\boldsymbol{u}^{r+1}$ and strains $d\varepsilon^{r+1}$.

Since the sub-matrices $\boldsymbol{K}_{nn}^{r+1}$ and $\boldsymbol{K}_{cn}^{r+1}$ are needed in the calculation of internal forces in the current iteration, the augmented tangential stiffness $\boldsymbol{K}_{ep,aug}^{r+1}$ for the $(r+1)$-th iteration is evaluated using the elasto-plastic stress-strain matrix $\boldsymbol{D}_{ep}^{r+1}$

$$\boldsymbol{K}_{ep,aug}^{r+1}=\int_V\boldsymbol{B}_{aug}^{T}\boldsymbol{D}_{ep}^{r+1}\boldsymbol{B}_{aug}dV \tag{16}$$

or

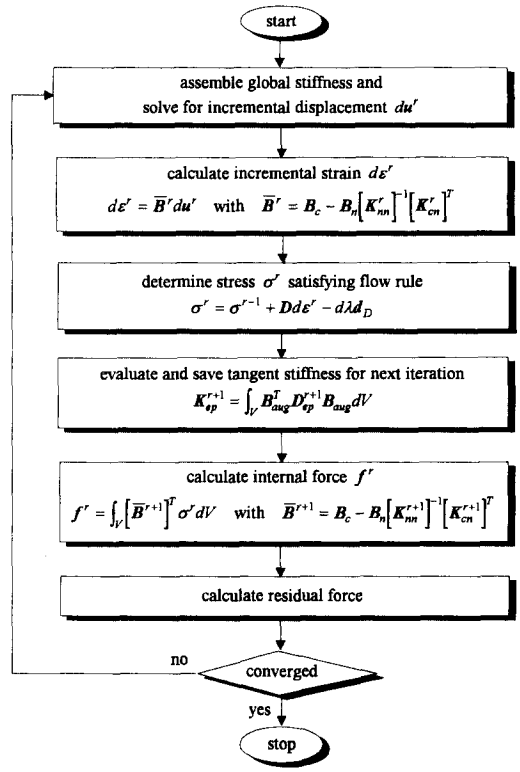

Fig. 2 Nonlinear iterative procedure for nonconforming element.

$$K_{ep,aug}^{r+1} = \begin{bmatrix} [K_{cc}^{r+1}] & [K_{cn}^{r+1}] \\ [K_{cn}^{r+1}]^T & [K_{nn}^{r+1}] \end{bmatrix} \tag{17}$$

in which B_{aug} denotes the augmented strain-displacement matrix $[B_c|B_n]$. Thus the stiffness of nonconforming elements for the new iteration is formed. With the processes described above, the iterative procedure for materially nonlinear analysis with nonconforming finite elements is shown in Fig. 2.

4. Numerical examples

Four numerical examples, *i.e.*, a cantilever beam, a clamped square plate, a solid under concentrated loading and a cut cube subject to inner pressure are presented to evaluate the validity and performance of the proposed elasto-plastic nonconforming solid element with variable nodes. The first two examples are selected to examine the nonlinear performance of the basic 8-node nonconforming element in flexure stress situations, and the other two examples to demonstrate the effectiveness of the variable-node element in the problems with local steep stress gradients. The influence of nonconforming modes included in the proposed element is carefully investigated in each example. Especially in the first two examples, the performance of the proposed eight node nonconforming element is compared with that of the quadratic Lagrange element with 27 nodes which is available in the general purpose nonlinear analysis program ADINA (1984).

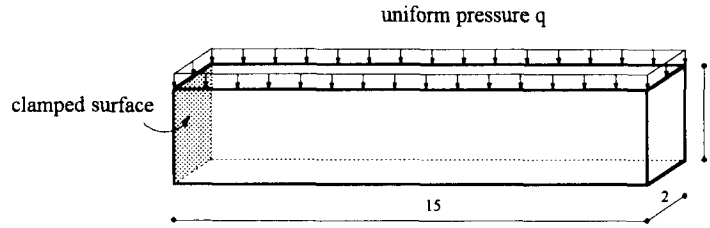

(a) Geometry and loading

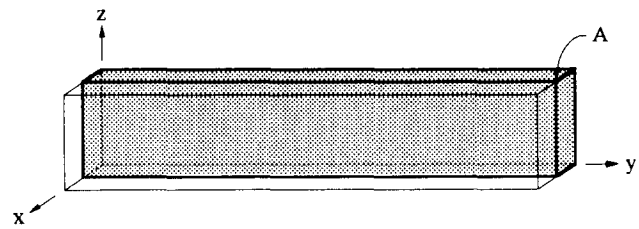

(b) Modelled portion : symmetric half

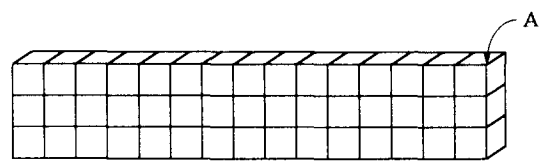

(c) Finite element mesh

Fig. 3 Cantilever beam

The same Gauss integration rule (3×3×3) as for the quadratic Lagrange element is used for the proposed element.

The stresses obtained with the element based on linear shape functions are recovered by a smoothing procedure in order to achieve more acceptable approximations. The superconvergent patch recovery (SPR) is employed in this study as a powerful and economic recovery technique (Zienkiewicz and Zhu 1992, Lee 1994). In each example, the elastic modulus of 29000 ksi is used with Poisson's ratio of 0.3. The effective stress-strain relationship of each material is taken to be elastic-perfectly plastic, and the yield stress σ_y of 36 ksi is used throughout.

4.1. Cantilever beam

A cantilever beam subject to a uniformly distributed load as shown in Fig. 3 is tested with three different types of elements; namely C8 (Conforming 8-node element), NC8 (NonConforming 8-node element) and L27 (Lagrange 27-node element). By taking advantage of symmetry, only a vertical half a beam is modelled and analyzed. The finite element model is composed of 45 elements and 300 degrees-of-freedom for 8-node elements (C8 and NC8) and 1680 for 27-node Lagrange element.

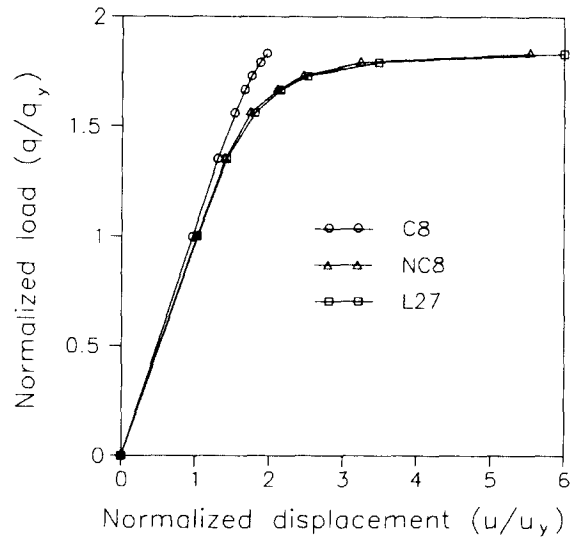

Fig. 4 Load-displacement relationship at beam tip

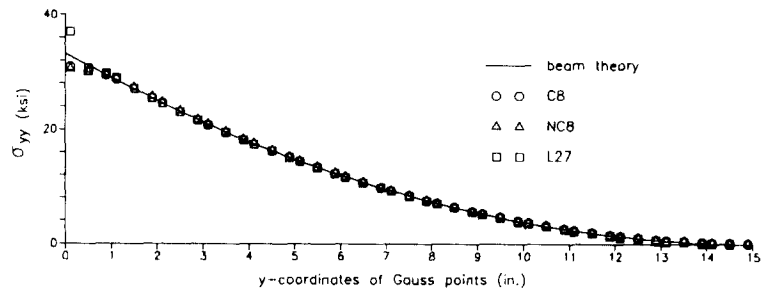

Fig. 5 Bending stress distribution at elastic stage (when $q=0.48$ ksi) (at $x=0.8873$ and $z=2.887$)

The variation of vertical displacement at the upper tip of symmetry plane (point A in Fig. 3) is shown in Fig. 4. For the purpose of an easy evaluation, the pressure load and the vertical displacement are normalized by the corresponding yield values obtained by simple bending theory ($q_y=0.48$ ksi and $u_y=0.0466$ in). It can be seen that the influence of nonconforming modes is significantly increased as the corresponding material goes into the inelastic range and that NC8 which has a much smaller number of degrees-of-freedom than L27 element provides almost the same accuracy of the nonlinear load-displacement relationship as L27. This figure also reveals that the use of conforming elements for the materially nonlinear analysis should not be recommended because of the poor performance in the nonlinear range.

The flexural stresses σ_{yy} at Gauss points nearest to the upper line of symmetry plane (at $x=0.8873$ and $z=2.887$) are shown in Fig. 5, at the first load step or at the elastic stage. The overall trends for each element type are similar to the reference values obtained by the beam theory. The effective stresses at the same Gauss points at the last load step (when $q=0.88$ ksi) are shown in Fig. 6 in which the similar yield pattern can also be seen for each element type. In this example, it is observed that the stress state is rather insensitive to the addition of non-

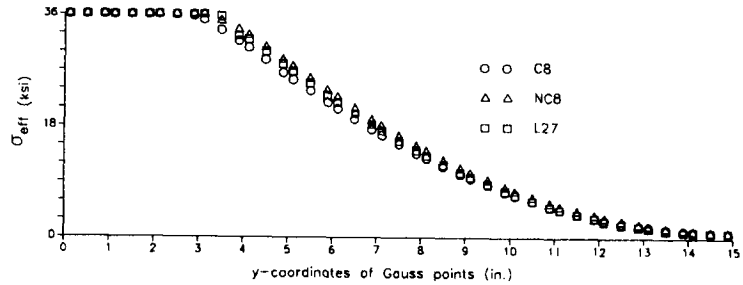

Fig. 6 Effective stress distribution at last load step (when $q=0.88$ ksi) (at $x=0.8873$ and $z=2.887$)

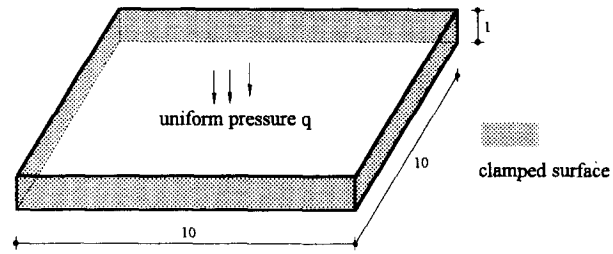

(a) Geometry and loading

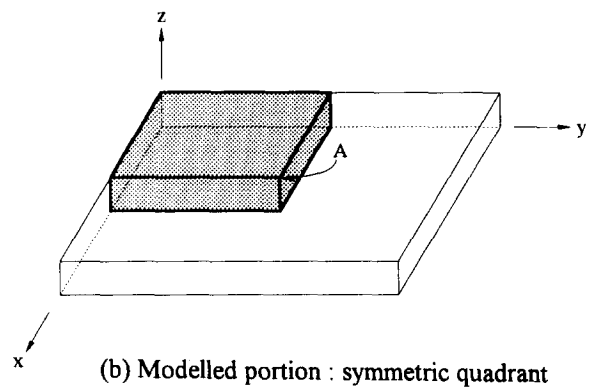

(b) Modelled portion : symmetric quadrant

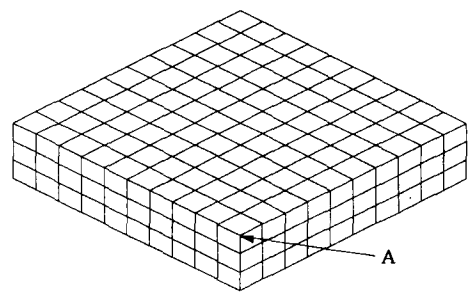

(c) Finite element mesh

Fig. 7 Clamped square plate

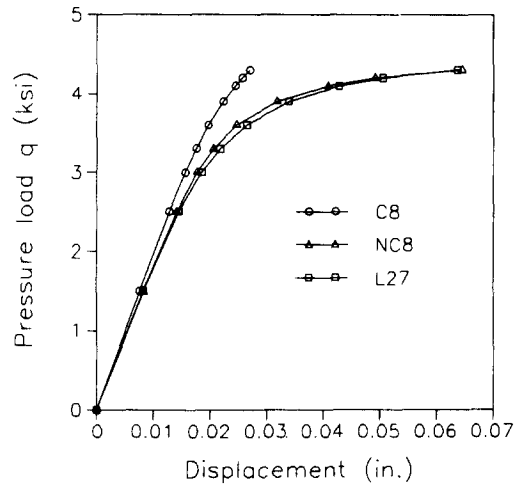

Fig. 8 Load-displacement relationship at mid-point

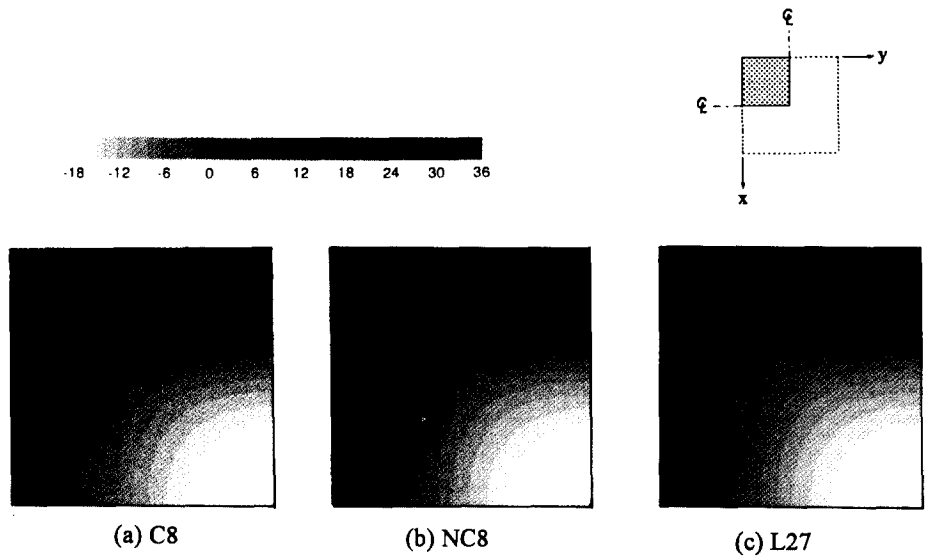

(a) C8 (b) NC8 (c) L27

Fig. 9 In-plane stress σ_{xx} contour at elastic stage (when $q=1.5$ ksi) (at $z=0.9628$)

conforming modes, whereas the bending behavior of the element is very sensitive to addition of nonconforming modes.

4.2. Clamped square plate

A clamped square plate subjected to a uniformly distributed load is examined, as shown in Fig. 7. By taking advantage of symmetry, only a quadrant of a plate is modelled and analyzed. The finite element model is composed of 300 elements and 1120 actual degrees-of-freedom for 8-node elements (C8 and NC8) and 8120 for 27-node element (L27). The vertical displacements at the upper point of the plate center (point A in Fig. 7) are shown in Fig. 8. Similar to the

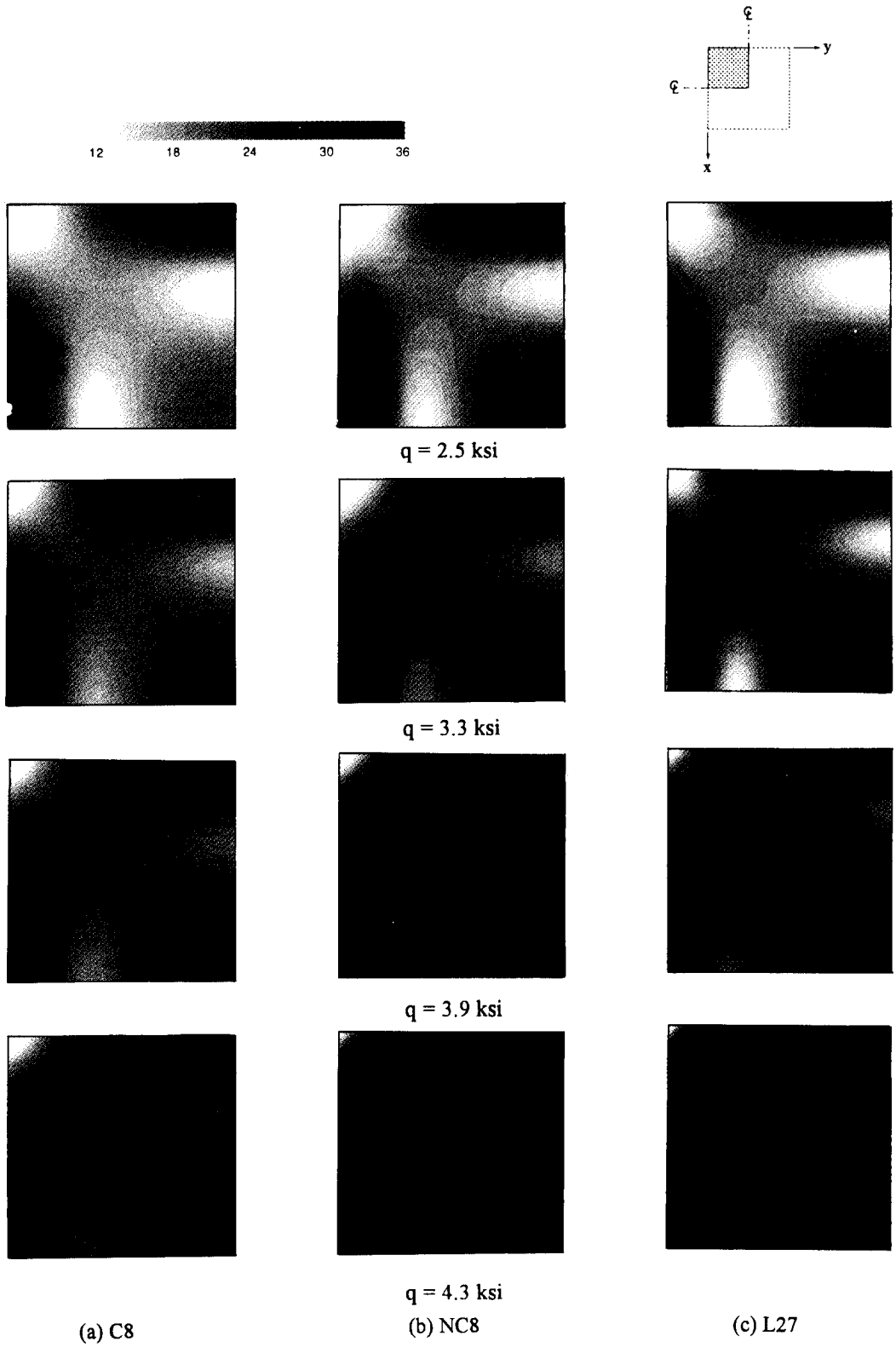

Fig. 10 Variation of effective stress contour (at $z=0.9628$)

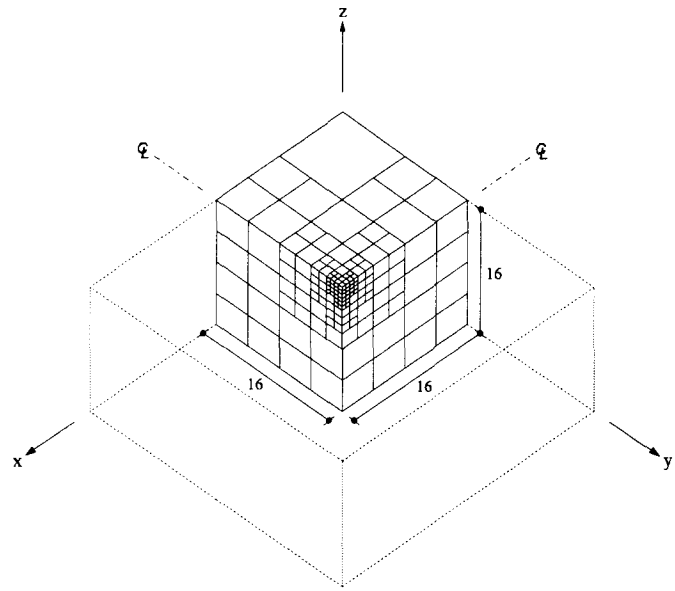

Fig. 11 Solid under concentrated loading

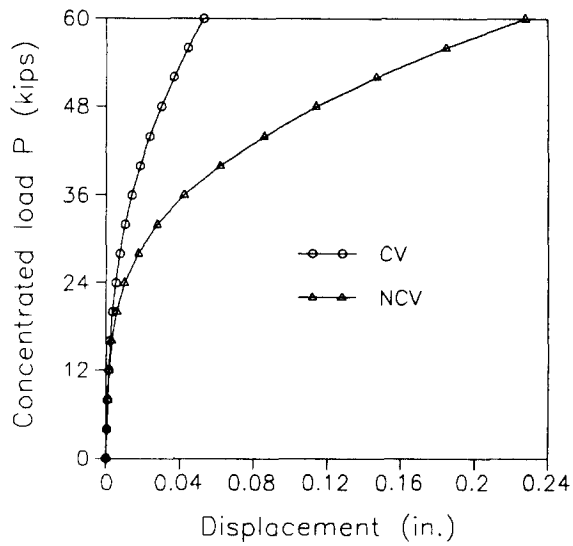

Fig. 12 Load-displacement relationship at loading point

previous beam problem, the influence of nonconforming modes is greatly increased as the corresponding material goes into the inelastic range and NC8 element provides almost the same accuracy of the nonlinear load-displacement relationship as the more complicated L27.

In Fig. 9, the contour map of the in-plane stress σ_{xx} at the upper Gauss points (at $z=0.9628$) under the initial load ($q=1.5$ ksi) is shown. The stress distributions for each element type, *i.e.*, C8, NC8 and L27, are of the similar pattern. In Fig. 10, the variation of effective stress contour at the same Gauss points under the different intensities of the distributed loads are shown.

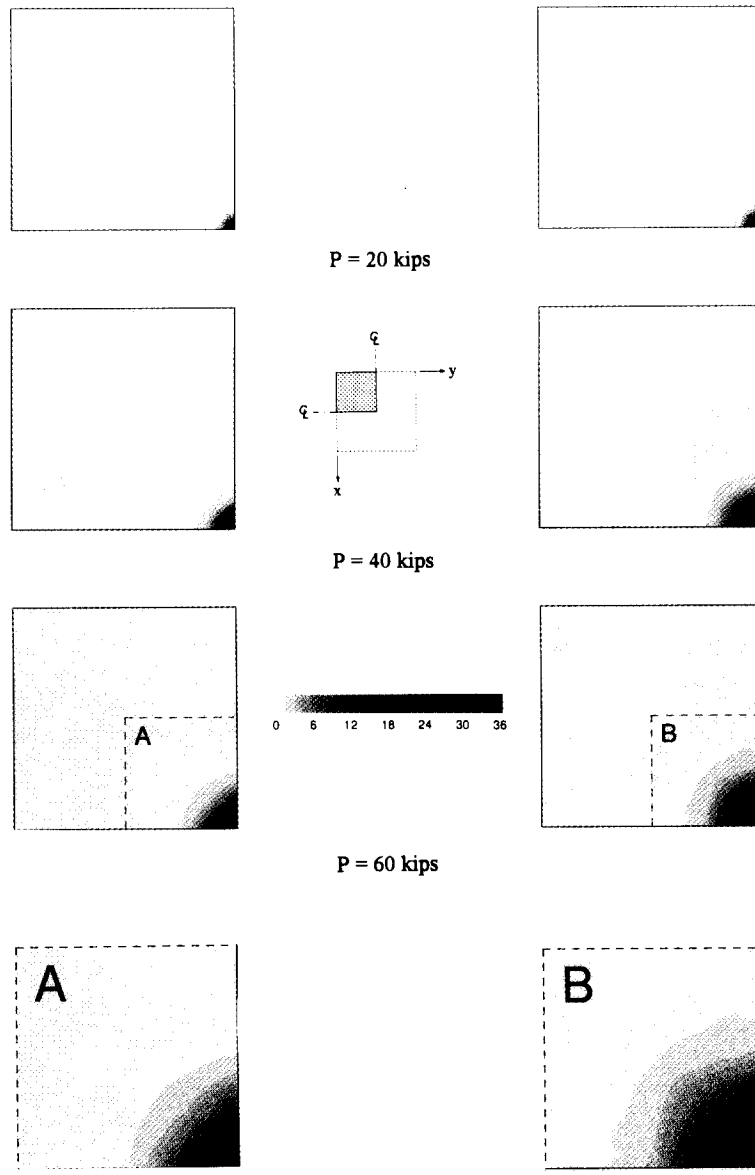

(a) CV (b) NCV

Fig. 13 Variation of effective stress contour at upper surface (at $z=16$)

The plastic zones are initiated at the center of plate edge and then developed at the plate center for each element type. As the corresponding material goes into the inelastic range, the yield zones propagate and a significant influence by the addition of nonconforming modes is also seen in this example. While the structure is fully plastified except the small corner zone at the final load step (when $q=4.3$ ksi) by the NC8 and L27 elements, some elastic zones still remain in the structure by C8. The progress of plastification in the structure can be more effectively

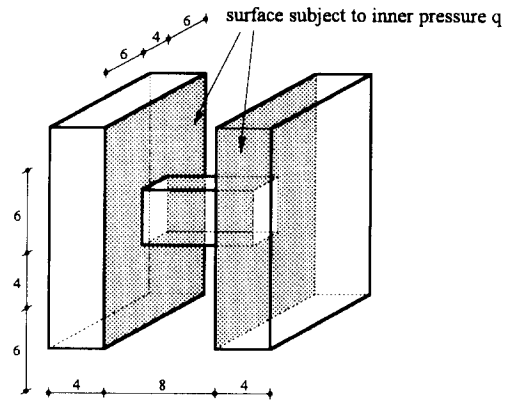

(a) Geometry and loading

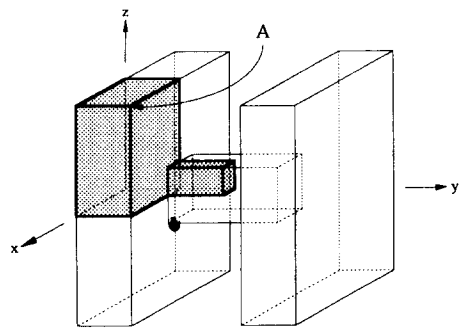

(b) Modelled portion: Symmetric eighth

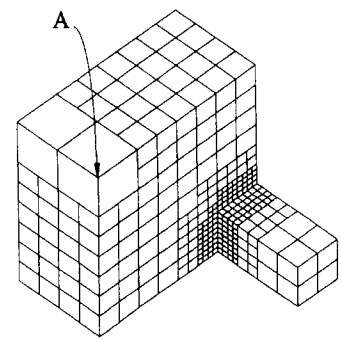

(c) Finite element mesh

Fig. 14 Cut cube subject to inner pressure

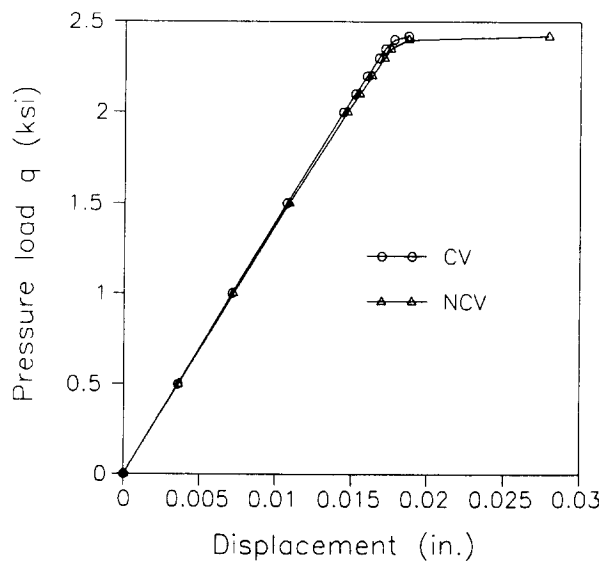

Fig. 15 Load-displacement relationship at corner point

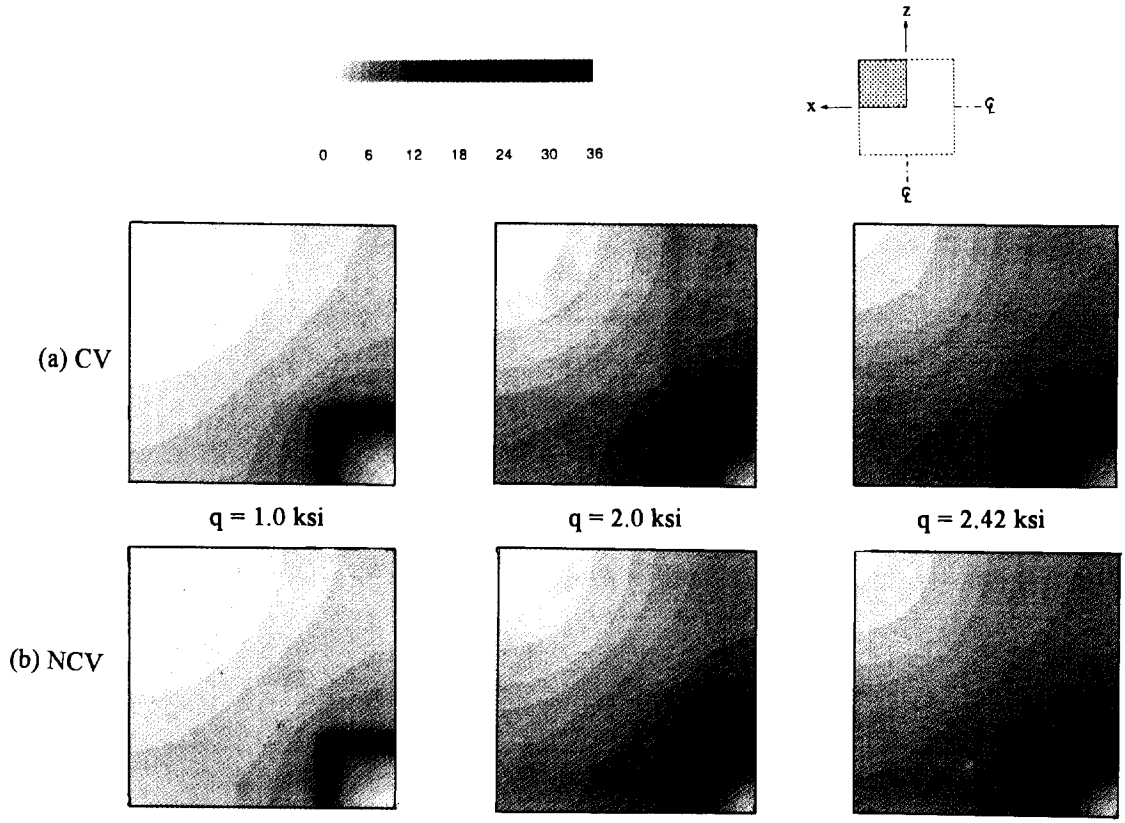

Fig. 16 Variation of effective stress contour at inner surface (at $y=4$)

detected either by the higher order element (L27) or by the nonconforming element (NC8).

4.3. Solid under concentrated loading

A solid clamped fully at the bottom surface and subjected to a concentrated load at the upper mid-point is examined, as shown in Fig. 11. A steep stress gradient is expected at the loading point and the local mesh refinement at this point is necessary for the effective and economic finite element analysis. By taking advantage of symmetry, only a quadrant of a solid is actually modelled and analyzed. The finite element model is composed of 190 elements and 919 actual degrees-of-freedom. The model utilizes the two different variable node transition elements, namely CV and NCV, and the basic behavior of the element is examined. L27 element is not used in this example since it utilizes a different local refinement scheme.

The variation of vertical displacement at the loading point is shown in Fig. 12, and the significant influence of nonconforming modes in inelastic range is assured again. In Fig. 13, the variation of effective stress contour at the upper surface (at $z=16$) is shown. A wider plastic zone is detected with the nonconforming element. It should be noted in this example that the yield zones do not propagate to the distant zone further due to the concentration of large increase of strain within a small zone near the loading point.

4.4. Cut cube subject to inner pressure

A cut cube subjected to inner pressure as shown in Fig. 14 is examined, by two different variable node transition elements, namely CV and NCV. Due to the abrupt change in geometry, a steep stress gradient is expected at the edges of connection between the large and small bodies and the local mesh refinement at these edges is required for the effective and economic finite element analysis. By taking advantage of symmetry, only one eighth of the total domain is actually modelled and analyzed. The finite element model in which both variable node transition elements are utilized is composed of 832 elements and 3861 degrees-of-freedom.

The variation of lateral displacement at the inner corner point (point A in Fig. 14) is shown in Fig. 15. It should be noted that failure in this example occurs abruptly by the concentrated yielding at inner edges. Thus the overall influence by the addition of nonconforming modes is smaller than the previous examples, except at the last load step where the load-displacement gradient is decreased abruptly. Fig. 16 shows the effective stress contour at the inner surface (at $y=4$), and the concentrated yielding at the inner edges can be seen. It is observed that the stress state as well as the displacement is rather insensitive to the addition of nonconforming modes since the normal stress is dominant and the flexural stress is negligible in this example.

5. Conclusions

The algorithm which uses the variable node nonconforming elements in the analysis of elasto-plastic problems has been established. Through the numerical tests, it is found that the influence of nonconforming modes is significantly increased as the material goes into the inelastic range. The bending behavior of the element is more sensitive to the addition of the nonconforming modes than the normal stress dominant case. Thus the nonconforming 8-node element (NC8) in an elasto-plastic analysis provides comparable results to those of the more complex quadratic Lagrange element (L27), even though the nonconforming element uses much less degrees-of-freedom.

Furthermore, the introduction of the variable nodes to the basic 8-node elements to establish the nonconforming transition elements (NCV) makes it possible to construct efficient and economic finite element meshes when steep stress gradient exists due to the abrupt change in geometry and/or loading. The most important strength of the element presented in this paper is such that in the elasto-plastic three-dimensional finite element analysis, it gives an economy in computation and a convenience in pre- and post-processing to achieve a required degree of accuracy. As the elasto-plastic iterative procedure was accomplished here for the general three-dimensional case, it could be easily applied without major modifications to the simpler cases such as membranes, plates and shells.

References

ADINA Engineering (1984), *ADINA-A finite element program for automatic dynamic incremental nonlinear analysis*, Report AE 84-1.

Chen, W.J. and Cheung, Y.K. (1992), "Three-dimensional 8-node and 20-node refined hybrid isoparametric elements", *Int. J. Num. Meth. Eng.*, **35**, 1871-1889.

Choi, C.K. and Lee, N.H. (1993), "Three dimensional transition solid elements for mesh gradation", *Structural Engineering and Mechanics*, **1**(1), 61-74.

Choi, C.K. and Park Y.M. (1989), "Nonconforming transition plate bending elements with variable mid-side nodes", *Comp. and Struc.*, **32**(2), 295-304.
Gupta, K.K. (1984), "Development of a solid hexahedron finite dynamic element", *Int. J. Num. Meth. Eng.*, **20**, 2143-2150.
Lee, N.H. (1994), "Three-dimensional adaptive mesh refinement using variable-node solid elements with nonconforming modes", *Ph. D. Thesis*, Korea Advanced Institute of Science and Technology.
Smith, I.M. and Kidger, D.J. (1992), "Elastoplastic analysis using the 14-node brick element family", *Int. J. Num. Meth. Eng.*, **35**, 1263-1275.
Spilker, R.L. and Singh, S.P. (1982), "Three-dimensional hybrid-stress isoparametric quadratic displacement element", *Int. J. Num. Meth. Eng.*, **18**, 445-465.
Owen, D.R.J. and Hinton, E. (1980), *Finite elements in plasticity*, Pineridge Press, Swansea.
Wilson, E.L. and Ibrahimbegovic, A. (1990), "Use of incompatible displacement modes for the calculation of element stiffnesses or stresses", *Finite Elements in Analysis and Design*, **7**, 229-241.
Yunus, S. M., Pawlak, T.P. and Cook, R.D. (1991), "Solid elements with rotational degrees of freedom: Part I-Hexahedron elements", *Int. J. Num. Meth. Eng.*, **31**, 573-592.
Zienkiewicz, O.C. and Zhu, J.Z. (1992), "The superconvergent patch recovery and a posteriori error estimates. Part 1: The recovery technique", *Int. J. Num. Meth. Eng.*, **33**, 1331-1364.

Appendix

The flow rule employed in this study is based on the following hypotheses (Owen and Hinton 1980):

(i) During any increment of stress, the changes of strain are assumed to be divisible into elastic and plastic components

$$d\varepsilon = d\varepsilon_e + d\varepsilon_p.$$

(ii) The yield criterion of von Mises is used to determine the stress level at which plastic deformation begins

$$f = k^2 - \frac{1}{3}\bar{\sigma}^2 = 0$$

where f is a yield function, k is a material parameter and $\bar{\sigma}$ is termed the effective stress.

(iii) With an associated theory of plasticity, the normality condition is assumed so that the plastic strain increment is proportional to the stress gradient of a yield function

$$d\varepsilon_p = d\lambda \frac{\partial f}{\partial \sigma}$$

where $d\lambda$ is termed the plastic multiplier.

From the assumptions and prerequisites mentioned above, the complete elasto-plastic incremental stress-strain relation can be obtained

$$d\sigma = \boldsymbol{D}_{ep} d\varepsilon$$

with

$$\boldsymbol{D}_{ep} = \boldsymbol{D} - \frac{\boldsymbol{d}_D \boldsymbol{d}_D^T}{H' + \boldsymbol{d}_D^T \boldsymbol{a}} \; ; \; \boldsymbol{d}_D = \boldsymbol{D}\boldsymbol{a}$$

where $\boldsymbol{a}$ is termed the flow vector

$$\boldsymbol{a}^T = \frac{\partial f}{\partial \sigma}$$

and the hardening parameter H' is obtained to be the local slope of the effective stress-plastic strain curve

$$H' = \frac{d\bar{\sigma}}{d\bar{\varepsilon}_p}$$

in which $\bar{\cdot}$ denotes the corresponding effective term.